PROTEIN STRUCTURE AND FOLDING:

Structural Analysis of the Y299C Mutant of *Escherichia coli* UDP-galactose 4-Epimerase: TEACHING AN OLD DOG NEW TRICKS

James B. Thoden, Jenny M. Henderson, Judith L. Fridovich-Keil and Hazel M. Holden

J. Biol. Chem. 2002, 277:27528-27534.
doi: 10.1074/jbc.M204413200 originally published online May 17, 2002

THE JOURNAL OF BIOLOGICAL CHEMISTRY
Vol. 277, No. 30, Issue of July 26, pp. 27528–27534, 2002

Printed in U.S.A.

Structural Analysis of the Y299C Mutant of *Escherichia coli* UDP-galactose 4-Epimerase

TEACHING AN OLD DOG NEW TRICKS*

Received for publication, May 6, 2002, and in revised form, May 16, 2002
Published, JBC Papers in Press, May 17, 2002, DOI 10.1074/jbc.M204413200

James B. Thoden‡, Jenny M. Henderson§¶, Judith L. Fridovich-Keil‖, and Hazel M. Holden‡**

From the ‡Department of Biochemistry, University of Wisconsin, Madison, Wisconsin 53706-1544 and the §Graduate Program in Nutrition and Health Sciences and the ‖Department of Human Genetics, Emory University School of Medicine, Atlanta, Georgia 30322

UDP-galactose 4-epimerase catalyzes the interconversion of UDP-Gal and UDP-Glc during normal galactose metabolism. The mammalian form of the enzyme, unlike its *Escherichia coli* counterpart, can also interconvert UDP-GalNAc and UDP-GlcNAc. One key feature of the epimerase reaction mechanism is the rotation of a 4-ketopyranose intermediate in the active site. By comparing the high resolution x-ray structures of both the bacterial and human forms of the enzyme, it was previously postulated that the additional activity in the human epimerase was due to replacement of the structural equivalent of Tyr-299 in the *E. coli* enzyme with a cysteine residue, thereby leading to a larger active site volume. To test this hypothesis, the Y299C mutant form of the *E. coli* enzyme was prepared and its three-dimensional structure solved as described here. Additionally, the Y299C mutant protein was assayed for activity against both UDP-Gal and UDP-GalNAc. These studies have revealed that, indeed, this simple mutation did confer UDP-GalNAc/UDP-GlcNAc converting activity to the bacterial enzyme with minimal changes in its three-dimensional structure. Specifically, although the Y299C mutation in the bacterial enzyme resulted in a loss of epimerase activity with regard to UDP-Gal by almost 5-fold, it resulted in a gain of activity against UDP-GalNAc by more than 230-fold.

Within recent years, the so-called short chain dehydrogenase/reductase (SDR)[1] superfamily has emerged as an important category of proteins and enzymes with more than 1600 examples being identified from a host of organisms (1). Typically, members of this superfamily catalyze oxidation-reduction type reactions with some functioning, for example, as dehydrogenases, dehydratases, isomerases, or epimerases (2–4). In most cases, enzymes belonging to this superfamily are typically around 250 amino acid residues in length and contain two characteristic signature sequences. The first of these is a Y*XX*K motif in which the conserved tyrosine plays a key role in catalysis. The second of the signature sequences is a G*XXX*G*X*G motif, which is located near the cofactor-binding pocket. Recently, on the basis of amino acid sequence homologies, it has been suggested that other members of the SDR superfamily may not function as enzymes or, at least, not in oxidation-reduction type capacities (5). One of these proteins, human TIP30, is a cofactor that enhances human immunodeficiency virus-1 Tat-activated transcription (6). Interestingly, TIP30 is 98% identical to human CC3, a protein associated with suppression of metastasis in small cell lung carcinomas (7). The recent and elegant structural analyses by Stammers *et al.* (8) have demonstrated that NmrA from *Aspergillus nidulans*, a negative transcriptional regulator, also belongs to the SDR protein superfamily.

One of the first members of the SDR protein superfamily to be extensively studied by high resolution x-ray crystallographic analyses was UDP-galactose 4-epimerase from *Escherichia coli*, which is somewhat larger with 338 amino acid residues per subunit (Ref. 9 and references therein). This dimeric enzyme functions in normal galactose metabolism by catalyzing the interconversion of UDP-Gal and UDP-Glc as indicated in Scheme 1. Within the last three years, the molecular architecture of the human form of the enzyme complexed with NADH and UDP-Glc has also been determined to high resolution (1.5 Å) and has led to the suggestion that Tyr-157 serves as the active site base required for catalytic activity (10). Both the bacterial and human epimerases are *B*-side-specific enzymes. As indicated in Fig. 1, the polypeptide chain of each subunit of human UDP-galactose 4-epimerase, hereafter referred to simply as epimerase, adopts a distinctly bilobal structure. The N-terminal domain is characterized by a seven-stranded, parallel β-sheet, whereas the smaller C-terminal domain contains six strands of β-sheet with five α-helices. The active site is wedged between the interface of these two domains.

Unlike the bacterial enzyme, human epimerase can interconvert UDP-GlcNAc and UDP-GalNAc as well UDP-Glc and UDP-Gal (11–15). Strikingly, however, the two enzymes are 55% identical with respect to amino acid sequence. A recent structural analysis of the human epimerase complexed with NADH and UDP-GlcNAc demonstrated that accommodation of the additional *N*-acetyl group at the C2 position of the sugar is accomplished by movement of the side chain of Asn-207 (16). Additionally, from this investigation it was shown that the active site volume of the human protein is ~15% larger than that observed for the *E. coli* enzyme.

The reaction mechanism of epimerase is thought to occur via the abstraction of the 4′-hydroxyl hydrogen of the sugar by the active site tyrosine, transfer of a hydride from C4 of the sugar to C4 of NAD^+ (*si*-face) to generate a 4′-ketopyranose interme-

* This work was supported in part by National Institutes of Health Grants DK47814 (to H. M. H.) and DK46403 (to J. L. F.-K.). The costs of publication of this article were defrayed in part by the payment of page charges. This article must therefore be hereby marked "*advertisement*" in accordance with 18 U.S.C. Section 1734 solely to indicate this fact.

The atomic coordinates and structure factors (code 1LRJ, 1LRK, and 1LRL) have been deposited in the Protein Data Bank, Research Collaboratory for Structural Bioinformatics, Rutgers University, New Brunswick, NJ (http://www.rcsb.org/).

¶ Supported in part by funds from National Institutes of Health Training Grant DK07734.

** To whom correspondence should be addressed. Tel.: 608-262-4988; Fax: 608-262-1319; E-mail: Hazel_Holden@biochem.wisc.edu.

[1] The abbreviation used is: SDR, short chain dehydrogenase/reductase.

diate and NADH, and finally rotation of the resulting 4′-ketopyranose moiety in the active site, thereby presenting the opposite face of the sugar to the reduced dinucleotide for subsequent hydride transfer back to the UDP-sugar substrate. A superposition of the human epimerase/NADH/UDP-GlcNAc structure onto the model of the bacterial enzyme with bound NADH and UDP-Glc is displayed in Fig. 2. Note that Cys-307 in the human enzyme is replaced with a tyrosine residue (Tyr-299) in the enzyme from *E. coli*. This substitution of the more bulky tyrosine residue in the active site of the bacterial enzyme could partly explain the inability of the *E. coli* enzyme to interconvert UDP-GlcNAc and UDP-GalNAc due to lack of the space required for rotation of the 4′-ketopyranose intermediate. To test this hypothesis, Tyr-299 in the *E. coli* enzyme was changed to a cysteine residue via site-directed mutagenesis. Here we present both enzymatic assays and high resolution x-ray crystallographic data demonstrating that replacement of Tyr-299 with a cysteine residue confers activity on the *E. coli* enzyme against UDP-GlcNAc and UDP-GalNAc with minimal structural perturbations.

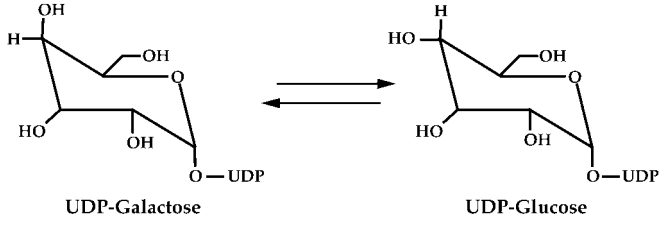

SCHEME 1

EXPERIMENTAL PROCEDURES

Construction of the Plasmid Containing the Y299C Mutation—The plasmid containing the epimerase Y299C mutation was constructed via cassette mutagenesis using the plasmid pTZSynE (17). The Y299C oligonucleotides were designed as follows: 1) Y299C-top, 5′-GGCGTGAAGGTGACCTTCCGGCGTGCTGGGCGGACG-3′ and 2) Y299C-bottom, 5′-CTAGCGTCCGCCCAGCACGCCGGAAGGTCACCTTCACGCCGC-3′ (Invitrogen). These oligonucleotides were utilized to give overhangs compatible with *Sac*II and *Nhe*I restriction sites at the 5′- and 3′-ends. They were boiled for 5 min and then slowly cooled to 4 °C to form the double-stranded cassette. The cassette was subsequently phosphorylated at the 5′-ends with polynucleotide kinase. The pTZSynE plasmid was digested with *Sac*II and *Nhe*I, treated with calf intestinal phosphatase, and purified with the GeneClean DNA purification kit. The mutagenic cassette was ligated into the cut pTZSynE plasmid with T4 DNA ligase.

Protein Purification and Crystallization—The wild-type and Y299C mutant epimerases were purified as previously described (18). Three different protein/NADH/UDP-sugar complexes were crystallized for this investigation, namely the complex of the wild-type enzyme with NADH and UDP-GlcNAc and the complexes of the Y299C protein with NADH and either UDP-GlcNAc or UDP-Glc. Note that attempts to solve the structures of the Y299C protein with NADH and either UDP-GalNAc or UDP-Gal resulted in either UDP-GlcNAc or UDP-Glc, respectively, being observed in the resulting electron density maps. Clearly the mutant enzyme is catalytically active in the crystalline state.

For the preparation of the above complexes, solid UDP-sugar was added to either the wild-type or Y299C protein samples to a final concentration of 20 mM. The samples were then allowed to stand at 4 °C

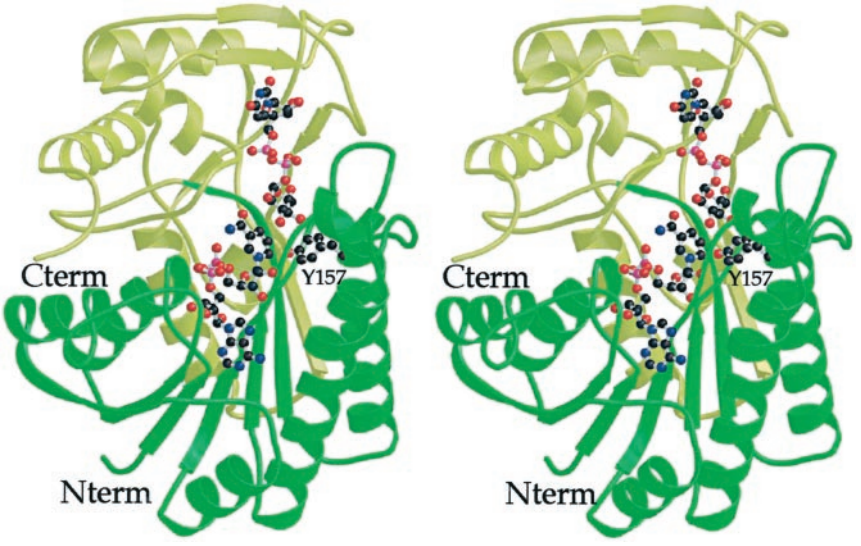

FIG. 1. **Ribbon representation of one subunit of human UDP-galactose 4-epimerase complexed with NADH and UDP-Glc.** The N- and C-terminal domains are displayed in *green* and *light green*, respectively, and the binding positions for the NADH and UDP-Glc molecules are indicated by the *ball-and-stick* models. Tyr-157 is the catalytic base that abstracts the 4′-hydroxyl hydrogen during the reaction mechanism. All figures were prepared with the software package, MOLSCRIPT (28).

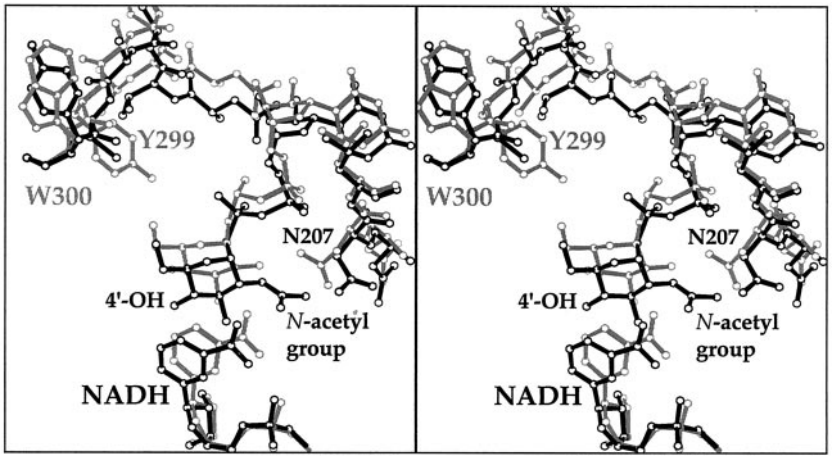

FIG. 2. **Superposition of the binding pockets for the UDP-sugars in the *E. coli* and human epimerases.** The human and bacterial enzymes are shown in *black* and *gray*, respectively. The structure of the bacterial enzyme was solved in the presence of UDP-Glc, whereas that of the human protein was determined in the presence of UDP-GlcNAc. Note that in the bacterial enzyme, Tyr-299 forms a hydrogen bond with either the 6′-hydroxyl of glucose (shown here) or the 2′-hydroxyl group of galactose (9).

TABLE I
X-ray data collection statistics

Complex	Resolution	Independent reflections	Completeness	Redundancy	Avg I/Avg	R_{sym}[a]
	Å		*%*		*σ(I)*	
Wild-type protein with UDP-GlcNAc	30.0 –1.75	42024	92.3	3.3	17.0	4.8
	1.83–1.75[b]	4851	81.4	1.8	2.0	35.6
Y299C protein with UDP-GlcNAc	30.0 –1.75	44201	94.7	3.9	13.9	5.5
	1.83–1.75[b]	5325	83.0	2.4	2.2	31.2
Y299C protein with UDP-Glc	30.0 –1.80	39438	93.1	3.6	14.7	5.4
	1.88–1.80[b]	4523	82.5	1.9	2.1	33.7

[a] $R_{sym} = (\Sigma|I-\bar{I}|/\Sigma I) \times 100$.
[b] Statistics for the highest resolution bin.

TABLE II
Relevant least-squares refinement statistics

Complex	Wild-type protein with UDP-GlcNAc	Y299C protein with UDP-GlcNAc	Y299C protein with UDP-Glc
Resolution limits (Å)	30.0–1.90	30.0–1.75	30.0–1.80
[a]*R*-factor (overall) %/no. reflections	19.5/33734	17.4/44201	19.5/39438
R-factor (working) %/no. reflections	19.2/30364	17.1/40001	19.4/35935
R-factor (free) %/no. reflections	26.8/3370	24.7/4420	26.1/3948
No. protein atoms	2635[b]	2632[c]	2625[d]
No. hetero-atoms	514[e]	640[f]	487[g]
Weighted root-mean-square deviations from ideality			
Bond lengths (Å)	0.016	0.015	0.015
Bond angles (deg)	2.37	2.29	2.46
Trigonal planes (Å)	0.006	0.007	0.007
General planes (Å)	0.016	0.013	0.013
Torsional angles (deg)[h]	16.5	15.4	15.5

[a] *R*-factor = $(\Sigma|F_O - F_C|/\Sigma|F_O|) \times 100$ where F_O is the observed structure-factor amplitude and F_C is the calculated structure-factor amplitude.
[b] These include multiple conformations for Thr-126 and Asp-232.
[c] These include multiple conformations for Gln-22, Lys-92, and Val-137.
[d] These include multiple conformations for Val-137 and Thr-144.
[e] These include 419 water molecules, 1 NADH, 1 UDP-GlcNAc, 2 sodium ions, and 1 tri-(ethylene glycol).
[f] These include 545 water molecules, 1 NADH, 1 UDP-GlcNAc, 2 sodium ions, and 1 tri-(ethylene glycol).
[g] These include 392 water molecules, 1 NADH, 1 UDP-Glc, 2 sodium ions, and 1 tri-(ethylene glycol).
[h] The torsional angles were not restrained during the refinement.

TABLE III
Enzymatic activity assays

Substrate	Enzyme	Specific activity	S.D.	n[a]
		mol product/mol active sites/sec		
UDP-Gal (0.41 mM)	Wild-type bacterial enzyme	23.9	11.0	16
	Wild-type human enzyme	33.8	11.2	17
	Y299C mutant enzyme	5.1	1.6	23
UDP-GalNAc (0.66 mM)	Wild-type bacterial enzyme	0.003	0.002	12
	Wild-type human enzyme	26.0	7.1	12
	Y299C mutant enzyme	0.69	0.13	18

[a] n, the number of separate analyses performed with aliquots of the indicated purified enzymes.

for 3 days. Following this incubation, they were dialyzed against 10 mM potassium phosphate (pH 8.0) and concentrated to 25 mg/ml.

Single crystals of all three complexes were grown by the hanging drop method of vapor diffusion at 4 °C. The precipitant was 15–19% polyethylene glycol 8000, 200 mM NaCl, and 100 mM HEPES (pH 7.5). Crystal growth generally required 4–7 days with crystals attaining maximum dimensions of 0.6 × 0.4 × 0.3 mm. All of the crystals belonged to the space group $P3_221$ with typical unit cell dimensions of $a = b = 83.2$ Å and $c = 109.5$ Å and one molecule per asymmetric unit.

X-ray Data Collection and Processing—Prior to x-ray data collection, the crystals were transferred to a cryoprotectant solution composed of 24% polyethylene glycol 8000, 600 mM NaCl, 20 mM UDP-sugar, 20% ethylene glycol, and 100 mM HEPES (pH 7.5). The crystals were suspended in 20-μm nylon loops and flash-cooled to −150 °C in a nitrogen gas stream. All x-ray data sets were collected with a HiStar (Bruker AXS) area detector system using CuK_α radiation generated from a Rigaku RU200 rotating anode generator operated at 50 kV and 90 mA and equipped with Supper long mirrors. The x-ray data were processed with SAINT (Bruker AXS, Inc.) and internally scaled with XSCALIBRE.[2] X-ray data collection statistics are presented in Table I.

Structure Determinations and Refinements—All of the structures were solved by Difference Fourier techniques employing the previously determined structure of the bacterial epimerase/NADH/UDP-Glc abortive complex (19) as the starting model. The coordinates for the solvents, UDP-sugars, and/or point mutation were removed from the starting models and rebuilt with TURBO (20) during the course of the least-squares refinements with the software package, TNT (21). Relevant refinement statistics are presented in Table II.

In Vitro Assays—Aliquots of each purified enzyme were stored in 50% glycerol with 4 mM NAD^+ in liquid nitrogen until needed. Assays to determine the level of epimerase activity with respect to UDP-Gal and UDP-GalNAc were performed essentially as previously described (11). Briefly, the conversion of UDP-Gal to UDP-Glc was measured in a 12.5-μl reaction containing 2.5 μl of premix (0.05 μCi of UDP-[^{14}C]Gal (Amersham Biosciences), 2 mM cold UDP-Gal, 0.2 M glycine buffer, pH 8.7), 2.5 μl of 20 mM NAD^+, and 7.5 μl of purified protein diluted in Johnston buffer (20 mM HEPES/KOH, pH 7.5, 1 mM dithiothreitol, and 0.3 mg of bovine serum albumin/ml). The amount of protein used per reaction ranged from 0.0001 to 0.005 μg, in order to stay within the predetermined linear range of the assay. Reactions were incubated at 37 °C for 30 min and were stopped by boiling at 100 °C for 10 min. Following high speed centrifugation for 15 min in a microcentrifuge, 10 μl of the sample was spotted onto a prewashed PEI-Cellulose TLC plate (Baker). After thorough drying, the plate was run for 16–24 h in a solvent containing 1.5 mM $Na_2B_4O_7$, 5 mM H_3BO_3, and 25% ethylene glycol. After running, plates were air-dried before being exposed to

[2] I. Rayment and G. Wesenberg, unpublished data.

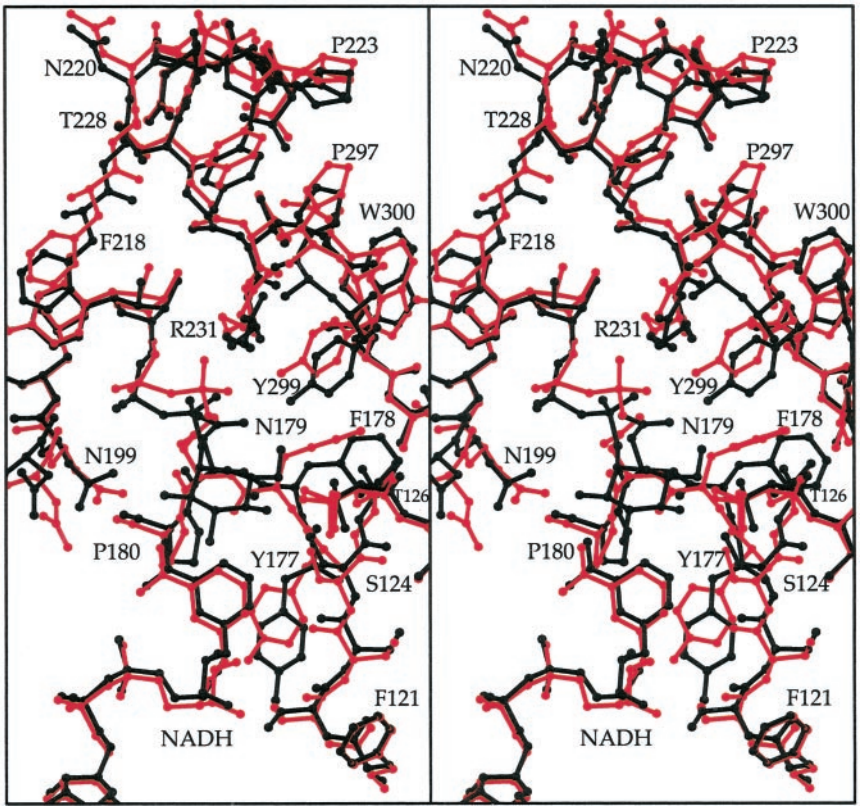

FIG. 3. **Superposition of the binding pockets for the wild-type *E. coli* epimerase with bound UDP-Glc or UDP-GlcNAc.** The structure of epimerase with bound UDP-Glc is shown in *black* and bound UDP-GlcNAc in *red*. The hexose portion of the UDP-GlcNAc is disordered in the electron density map and hence is not included in this figure. Note that Thr-126 adopts multiple conformations in the enzyme/NADH/UDP-GlcNAc complex. For the sake of clarity, ordered solvent molecules were not included in this figure.

storage phosphor screens (Amersham Biosciences) overnight. Images were visualized with a Typhoon 9200 variable mode imager and quantified using ImageQuant software (both from Amersham Biosciences). Percent conversion was determined by dividing the product signal by the total signal and multiplying by 100. This number was converted to specific activity using the formula: ((% conversion/100) × 5.085 nmol of substrate)/(μg of enzyme × 30 min).

The conversion of UDP-GalNAc to UDP-GlcNAc was determined essentially as described above, with the following assay components per 25 μl of reaction: 8.75 μl of premix (0.04 μCi of UDP-[^{14}C]GalNAc (ICN), 1.89 mM cold UDP-GalNAc, 28.6 mM pyruvate, 286 mM glycine, pH 8.7, 5 μl of 20 mM NAD) and 11.25 μl of protein diluted in Johnston buffer. The amount of protein used in each assay ranged from 0.0005 to 2.0 μg. Assays were performed as for UDP-Gal, with a TLC run-time of 10 h and quantified as described for UDP-Gal. The percentage conversion was translated to specific activity using the following formula: ((% conversion/100) × 16.52909 nmol of substrate)/(μg of enzyme × 30 min).

RESULTS AND DISCUSSION

To confirm the difference in substrate specificities of the wild-type human and *E. coli* epimerases, as well as to define the catalytic impact of the Y299C mutation in the bacterial enzyme, *in vitro* enzymatic activity analyses were conducted with purified proteins and each of the substrates in question, UDP-Gal and UDP-GalNAc. With regard to the wild-type human and *E. coli* enzymes, the results presented in Table III clearly confirm earlier reports (11–15, 22–24) indicating that although human UDP-galactose 4-epimerase demonstrates strong activity against both substrates, the bacterial enzyme is active only against UDP-Gal. Indeed, the wild-type bacterial enzyme is more than 8,000-fold less active against UDP-GalNAc than it is against UDP-Gal. In contrast, the Y299C bacterial enzyme demonstrated significant activity against both substrates (Table III). Although the Y299C mutation in the bacterial enzyme resulted in a loss of epimerase activity with regard to UDP-Gal by almost 5-fold, it resulted in a gain of activity with regard to UDP-GalNAc by 230-fold.

As a control experiment, the first complex to be solved in this combined structural and functional investigation was that of the wild-type bacterial enzyme with bound NADH and UDP-GlcNAc. In light of past x-ray crystallographic studies of the binding of UDP-sugar moieties such as UDP-mannose or UDP-4-deoxy-4-fluoro-α-D-galactose to *E. coli* epimerase (25), it was anticipated *a priori* that little conformational change would accompany the binding of UDP-GlcNAc in the active site of the wild-type enzyme. In retrospect that assumption was perhaps naïve in that the ligand, UDP-GlcNAc, contains a rather bulky group attached to C2 of the hexose. The electron density corresponding to the sugar moiety is indeed disordered in the map, thus indicating that it adopts multiple conformations when bound in the epimerase active site. The electron density corresponding to the UDP portion of the ligand is unambiguous, however. Additionally, the electron density corresponding to the polypeptide chain between Asn-131 and Ile-134 is weak.

There are several regions in the polypeptide chain that change in the presence of UDP-GlcNAc *versus* UDP-Glc, as can be seen by the superposition displayed in Fig. 3. Indeed, the α-carbons for the epimerase/NADH/UDP-Glc and epimerase/NADH/UDP-GlcNAc models superimpose with a root-mean-square deviation of 0.52 Å. Most of the changes are confined primarily to the regions delineated by Phe-121 to Asn-131, Tyr-177 to Pro-180, Gln-194 to Leu-200, Phe-218 to Arg-231, and Arg-292 to Asp-302. All of these regions contain either side chains or backbone atoms that participate in hydrogen-bonding interactions with the UDP-sugars and, thus, are sensitive to the chemical identity of the ligand positioned in the active site. In the previously determined wild-type epimerase/NADH/UDP-Glc model, for example, O^{γ} of Ser-124 lies within 2.6 Å of the 4′-hydroxyl group of the glucose moiety, while the side chains for both Asn-179 and Tyr-299 form hydrogen bonds with the 6′-hydroxyl group of glucose (9).

The movement of the side chain carboxamide group of Asn-199, as shown in Fig. 3, is especially striking. When UDP-Glc is bound in the active site, both the 2′-hydroxyl group of the sugar and an α-phosphoryl oxygen are hydrogen-bonded to $N^{\delta 2}$ of

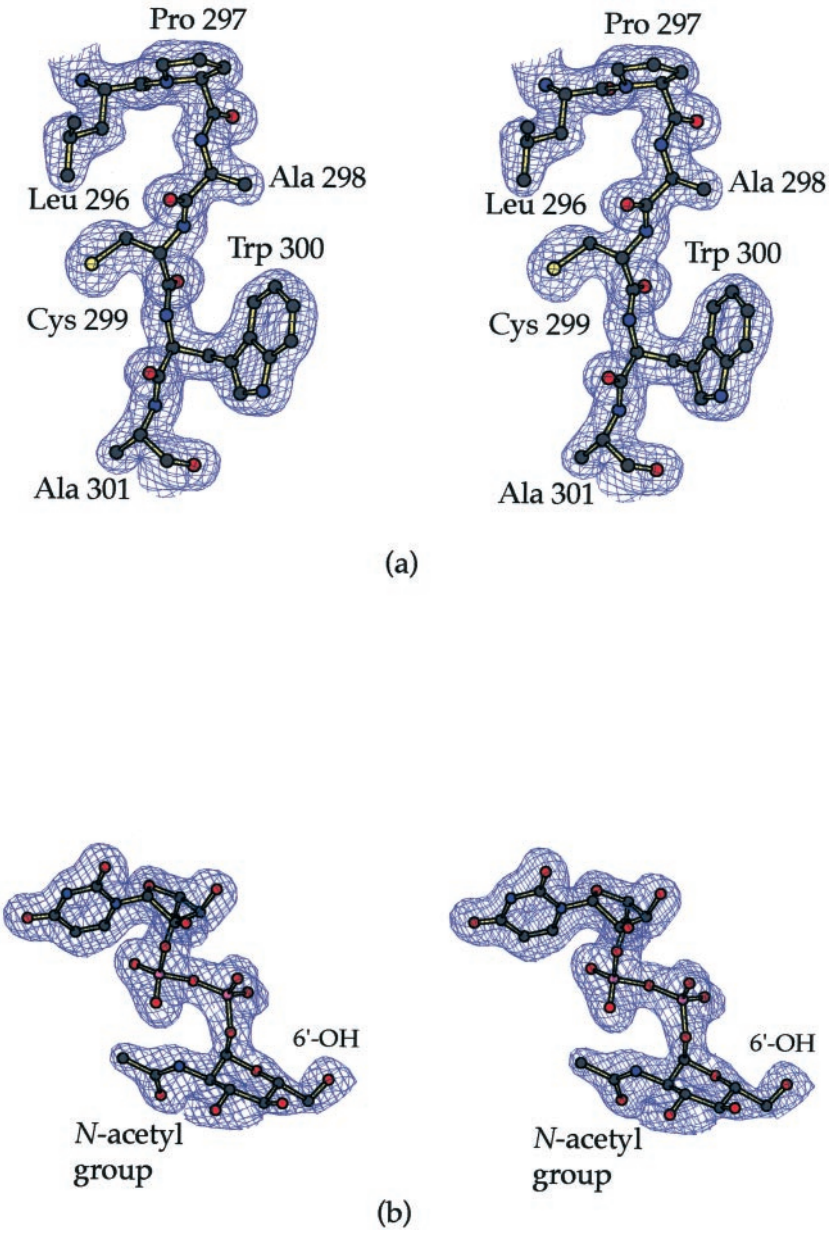

FIG. 4. **Representative electron density for the Y299C enzyme/NADH/UDP-GlcNAc complex.** *a*, electron density near the region of the mutation. The map was contoured at 1σ and calculated with coefficients of the form $(2F_o - F_c)$ where F_o was the native structure factor amplitude and F_c was the calculated structure factor amplitude. *b*, the electron density corresponding to the UDP-GlcNAc ligand. This map was contoured at 2σ and calculated with coefficients of the form $(F_o - F_c)$ where F_o was the native structure factor amplitude and F_c was the calculated structure factor amplitude. Note that the ligand had not been built into the electron density when this map was calculated.

Asn-199. However, with UDP-GlcNAc bound in the active site, this interaction is missing, and the side chain of Asn-199 rotates toward the nicotinamide ring of NADH. There is a general shift of ~0.4 Å of the nucleoside portions of UDP-GlcNAc *versus* UDP-Glc in the active site. The lack of activity of the *E. coli* epimerase against UDP-GlcNAc or UDP-GalNAc most likely arises from the following two key factors: (*a*) the inability of the larger sugar moiety to correctly position into the active site and (*b*) the inability of the 4′-ketopyranose intermediate to rotate in the active site.

The second structure that was solved in this investigation was that of the Y299C mutant protein complexed with NADH and UDP-GlcNAc. The electron density corresponding to the region surrounding the mutation is well ordered, as displayed in Fig. 4*a*. In fact, the molecular changes that occur upon substituting a cysteine residue for Tyr-299 are localized in the regions defined by Arg-176 to Asn-179, Ala-216 to Arg-231, and His-287 to Cys-299. The net effect of these changes, as indicated in Fig. 5*a*, is an opening of the substrate binding cleft, which results in an overall 20% increase in the volume of the active site for the Y299C mutant protein as calculated with the program VOIDOO (26, 27). The α-carbons for the wild-type enzyme with bound UDP-Glc and the Y299C mutant protein with bound UDP-GlcNAc correspond with a root-mean-square deviation of 0.96 Å.

A portion of the electron density map corresponding to the bound UDP-GlcNAc in the Y299C mutant protein is depicted in Fig. 4*b* and, unlike that observed for the wild-type protein/NADH/UDP-GlcNAc complex, the sugar moiety is reasonably well ordered. Average *B*-factors for the NADH and the UDP-GlcNAc ligands are 22.0 and 43.6 Å^2, respectively. A close-up view of the active site for the Y299C mutant protein is displayed in Fig. 5*b*. In the case of the wild-type bacterial epimerase, the side chain functional groups of Asn-179, Asn-199, and Tyr-299 form hydrogen-bonding interactions with the hexose sugar moieties of the UDP-Glc or UDP-Gal substrates. Additionally, O^{γ} of Ser-124 lies within 2.6 Å of the 4′-hydroxyl group of the glucose moiety in UDP-Glc. As can be seen in Fig. 5*b*, the UDP-GlcNAc ligand is situated in the active site such that these residues are no longer within hydrogen-bonding distance to the hydroxyl groups of the hexose. Indeed, the sugar hydroxyl groups lie only within hydrogen-bonding distance to

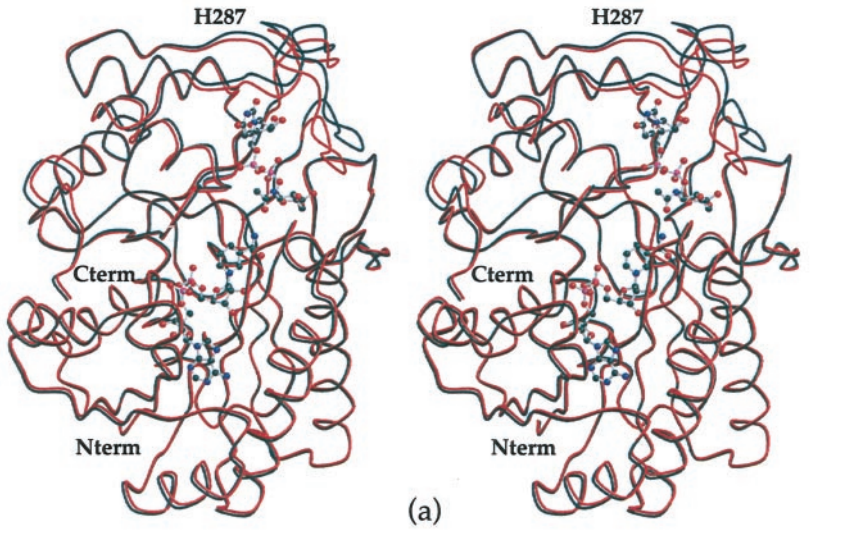

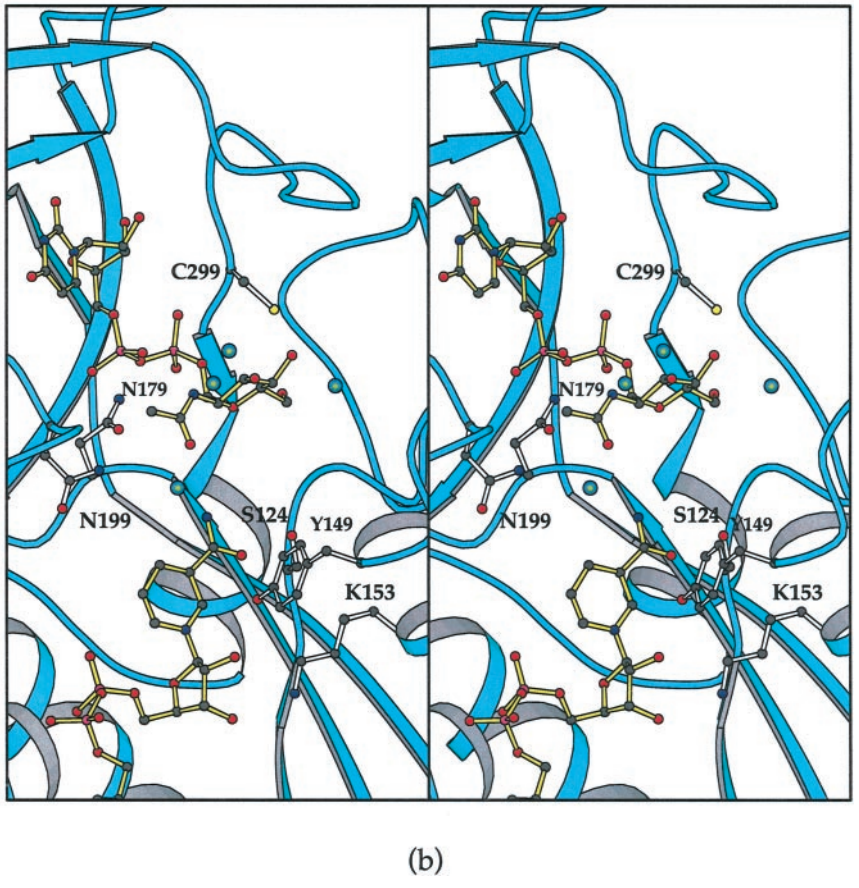

FIG. 5. **Structure of the Y299C enzyme/NADH/UDP-GlcNAc complex.** *a*, a superposition of the α-carbons for the wild-type enzyme with bound NADH and UDP-Glc in *red* and the Y299C enzyme/NADH/UDP-GlcNAc complex in *black*. The NADH and UDP-GlcNAc ligands for the mutant protein are displayed in *ball-and-stick* representations. *b*, a close-up view of the active site, in the context of secondary structure. For the sake of clarity, only those amino acid side chains in the wild-type enzyme that are important for anchoring the hexose moiety to the protein are shown, namely Asn-179 and Asn-199. Ordered water molecules are depicted in *yellow-blue* gradients. Also included are those residues thought to play critical roles in the reaction mechanism of epimerase, namely Lys-153, Tyr-149, and Ser-124.

solvent molecules. In the wild-type protein/NADH/UDP-Glc model, the nicotinamide ring of the cofactor is in the *syn*-conformation as would be expected for a *B*-side-specific enzyme. In the Y299C mutant protein/NADH/UDP-GlcNAc model, the nicotinamide ring is in the *anti*-conformation such that the carbonyl oxygen of its carboxamide group lies within 2.5 Å from O^{γ} of Ser-124. The distance between the C4 carbon of the *N*-acetylglucosamine moiety and the C4 carbon of the nicotinamide ring is 9.4 Å. In the wild-type enzyme/NADH/UDP-Glc complex, this distance is 3.8 Å. The fact that the mutant protein but not the wild-type bacterial enzyme is active against UDP-GalNAc as a substrate argues for the fact that in the mutant protein the UDP-sugar must, at some point, rotate into the proper position for catalysis.

The final structure to be solved in this investigation was that of the Y299C mutant protein complexed with NADH and UDP-Glc. The electron density corresponding to the hexose portion of the UDP-Glc was weak. This is in sharp contrast to that observed for the wild-type enzyme/NADH/UDP-Glc crystalline complex (19). The α-carbons for the wild-type and Y299C pro-

FIG. 6. **Structure of the Y299C enzyme/NADH/UDP-Glc complex.** The UDP-Glc and NADH in the Y299C enzyme are displayed in *filled yellow bonds*. For the sake of comparison, the positions of Tyr-299 and the UDP-Glc ligand in the wild-type enzyme are indicated by *pink filled bonds*. In the wild-type protein, Tyr-299 plays a key role in substrate binding by hydrogen-bonding to the 6′-hydroxyl group of the glucose moiety (*dashed line*).

teins complexed with NADH and UDP-Glc correspond with a root-mean-square deviation of 0.56 Å. For comparison, the α-carbons for the mutant proteins that were complexed with either UDP-Glc or UDP-GlcNAc superimpose with a root-mean-square deviation of 0.22 Å. A close-up view of the Y299C mutant protein active site with NADH and UDP-Glc is shown in Fig. 6. In this complex, the nicotinamide ring of the NADH ligand is in the *syn*-conformation. The position of the glucose moiety is approximate because of the weakness of the electron density. It is clear, however, that in the Y299C mutant protein the loss of the hydrogen bond between Tyr-299 and the 6′-hydroxyl group of glucose normally observed in the wild-type enzyme results in a movement of the sugar away from the nicotinamide ring. The 5-fold reduction in enzymatic activity of this Y299C mutant protein arises in part because of the loss of this electrostatic interaction, thereby leading to unproductive binding modes for the hexose portion of the UDP-sugar substrate.

In conclusion, by comparing the three-dimensional structures of both the human and bacterial UDP-galactose 4-epimerases, it was possible to predict the necessary single site-specific change that would be required to confer UDP-GlcNAc/UDP-GalNAc interconverting activity on the *E. coli* protein. This combined structural/functional analysis emphasizes the power in comparing in detail various superfamily members for the rational design of new enzymatic activities on particular protein scaffolds.

Acknowledgments—We thank Sandra Harding for determining the initial crystallization conditions of the Y299C protein/NADH/UDP- GlcNAc complex. We also thank Drs. Dale Edmondson and Paige Newton-Vinson for generously allowing and helping us to use their fermenter.

REFERENCES

1. Oppermann, U. C. T., Filling, C., and Jörnvall, H. (2001) *Chem. Biol. Interact.* **130–132,** 699–705
2. Jörnvall, H., Persson, B., Krook M., Atrian, S., González-Duarte, R., Jeffery, J., and Ghosh, D. (1995) *Biochemistry* **34,** 6003–6013
3. Duax, W. L., Griffin, J. F., and Ghosh, D. (1996) *Curr. Opin. Struct. Biol.* **6,** 813–823
4. Duax, W. L., Ghosh, D., and Pletnev, V. (2000) *Vitam. Horm.* **58,** 121–148
5. Baker, M. E. (1999) *Curr. Biol.* **9,** R471
6. Xiao, H., Tao, Y., Greenblatt, J., and Roeder, R. G. (1998) *Proc. Natl. Acad. Sci. U. S. A.* **95,** 2146–2151
7. Shtivelman, E. (1997) *Oncogene* **14,** 2167–2173
8. Stammers, D. K., Ren, J., Leslie, K., Nichols, C. E., Lamb, H. K., Cocklin, S., Dodds, A., and Hawkins, A. R. (2001) *EMBO J.* **20,** 6619–6626
9. Thoden, J. B., and Holden, H. M. (1998) *Biochemistry* **37,** 11469–11477
10. Thoden, J. B., Wohlers, T. M., Fridovich-Keil, J. L., and Holden, H. M. (2000) *Biochemistry* **39,** 5691–5701
11. Wohlers, T. M., Christacos, N. C., Harreman, M. T., and Fridovich-Keil, J. L. (1999) *Am. J. Hum. Genet.* **64,** 462–470
12. Maley, F., and Maley, G. F. (1959) *Biochim. Biophys. Acta* **31,** 577–578
13. Piller, F., Hanlon, M. H., and Hill, R. L. (1983) *J. Biol. Chem.* **258,** 10774–10778
14. Kingsley, D. M., Kozarsky, K. F., Hobbie, L., and Krieger, M. (1986) *Cell* **44,** 749–759
15. Wohlers, T. M., and Fridovich-Keil, J. L. (2000) *J. Inherit. Metab. Dis.,* **23,** 713–729
16. Thoden, J. B., Wohlers, T. M., Fridovich-Keil, J. L., and Holden, H. M. (2001) *J. Biol. Chem.* **276,** 15131–15136
17. Liu, Y., Thoden, J. B., Kim, J., Berger, E., Gulick, A. M., Ruzicka, F. J., Holden, H. M., and Frey, P. A. (1997) *Biochemistry* **36,** 10675–10684
18. Thoden, J. B., Frey, P. A., and Holden, H. M. (1996) *Biochemistry* **35,** 2557–2566
19. Thoden, J. B., Frey, P. A., and Holden, H. M. (1996) *Biochemistry* **35,** 5137–5144
20. Roussel, A., and Cambillau, C. (1991) *Silicon Graphics Geometry Partners Directory*, Silicon Graphics, Menlo Park, CA
21. Tronrud, D. E., Ten Eyck, L. F., and Matthews, B. W. (1987) *Acta Crystallogr. Sect. A.* **43,** 489–501
22. Darrow, R. A., and Rodstrom, R. (1968) *Biochemistry* **7,** 1645–1654
23. Salo, W. L., Nordin, J. H., Peterson, D. R., Bevill, R. D., and Kirkwood, S. (1968) *Biochem. Biophys. Acta* **151,** 484–492
24. Kingsley, D. M., Krieger, M., and Holton, J. B. (1986) *N. Eng. J. Med.* **314,** 1257–1258
25. Thoden, J. B., Hegeman, A. D., Wesenberg, G., Frey, P. A., and Holden, H. M. (1997) *Biochemistry* **36,** 6294–6304
26. Kleywegt, G. J., and Jones, T. A. (1993) *Newsl. Prot. Crystallogr.* **29,** 26–28
27. Kleywegt, G. J., and Jones, T. A. (1994) *Acta Crystallogr. Sect. D. Biol. Crystallogr.* **50,** 178–185
28. Kraulis, P. J. (1991) *J. Appl. Cryst.,* **24,** 946–950